Proceedings of the Institute of Acoustics

THE INFLUENCE OF WALL FLEXIBILITY ON SOUND PROPAGATION IN A DUCT WITH BULK-REACTING LINERS

A. Cummings(1), R.J. Astley(2) and N. Sormaz(1)

(1)Department of Engineering Design and Manufacture, University of Hull, Hull HU6 7RX
(2)Department of Mechanical Engineering, University of Canterbury, Christchurch, New Zealand.

1. INTRODUCTION

Sound attenuation in rigid ducts with bulk-reacting, sound-absorbent porous liners or splitters has been fairly extensively studied both in the absence and presence of mean gas flow in the space(s) between the absorbent layer (see, for example, references [1-3]). Moreover, the influence of wall motion on sound propagation in rectangular ducts with flexible walls has been examined [4], in a study of noise "breakout" from ductwork, and it has also been shown [5] that structural/acoustic wave combinations exist wherein the energy flow can concentrate itself predominantly either in the structure or in the fluid in the duct.

No efforts appear to have been made to determine the effects of wall motion on sound attenuation processes in flexible-walled lined ducts. In the analysis of sound attenuation in acoustically lined sheet metal air-moving ductwork or package silencers, it is of considerable importance to know how wall flexibility affects both the attenuation process itself and the distribution of energy flow in the structure and in the fluid contained in the duct, particularly where axial discontinuities ("structural" or "geometrical") exist.

In this paper, some of the effects of wall flexibility on sound attenuation in ducts having bulk liners are examined. A finite element (FE) structural and acoustic model is described, and experimental results are compared to numerical data.

2. THEORY.

2.1 Geometry and governing equations.

The geometry of the problem to be investigated is illustrated in figure 1a. A prismatic duct lies along the z axis of a cartesian coordinate system. Its cross section consists of an airway (region R_0) and an acoustically absorbent liner (region R_a). The wall of the duct is rigid except for a thin elastic plate adjacent to the liner (contour C_3 in figure 1b). The acoustical pressure in the duct, $p^*(\mathbf{x},t)$, and the lateral displacement of the plate, $u^*(s,z,t)$, vary harmonically with time so that

$$p^*(\mathbf{x},t)=p'(\mathbf{x})e^{i\omega t} \quad \text{and} \quad u^*(s,z,t)=u'(s,z)e^{i\omega t}$$

The acoustical equation in the duct is then

$$\nabla^2 p' + k^2 p' = 0 \text{ , where } k = k_0 \text{ (real, } = \Omega/c_0) \text{ in the airway, } = k_a \text{ (complex) in the liner .} \quad (1)$$

The time harmonic version of the unsteady plate equation is

$$g(\partial^2/\partial s^2 + \partial^2/\partial z^2)^2 u' - q\Omega^2 u' = p', \text{ on } C_3, \quad (2)$$

where 'g' is the flexural rigidity of the plate and 'q' its mass per unit area. The pressure and displacement are further coupled through the kinematic constraint on C_3 which requires

$$(1/\rho_a \Omega^2)\, \underline{\nabla} p' . \mathbf{n}_3 = u' \text{ on } C_3, \quad (3)$$

(ρ_a is the a complex density for the liner consistent with the choice of a complex wavenumber k_a). Boundary conditions on the duct perimeter and at the interface between the airway and liner are:

$$\underline{\nabla} p' . \mathbf{n}_1 = 0 \text{ on } C_1 \quad \text{(rigid wall)}, \quad (4)$$

$$p'_o = p'_a \text{ on } C_2, \quad \text{(continuity of pressure)}, \quad (5)$$

$$\text{and } (1/\rho_o \Omega^2)[\underline{\nabla} p'_o . \mathbf{n}_2] = (1/\rho_a \Omega^2)[\underline{\nabla} p'_a . \mathbf{n}_2] \text{ on } C_2 \text{ ,} \quad (6)$$

(continuity of particle displacement).

(note: p'_a and p'_o denote acoustic pressure in R_a and R_o).

2.2. Formulation of the eigenvalue problem.
Solutions for u' and p' are now sought which have the form

$$p'(\mathbf{x}) = p(x,y)e^{-i\alpha z} \quad \text{and} \quad u'(s,z) = u(s)e^{-i\alpha z}. \quad (7)$$

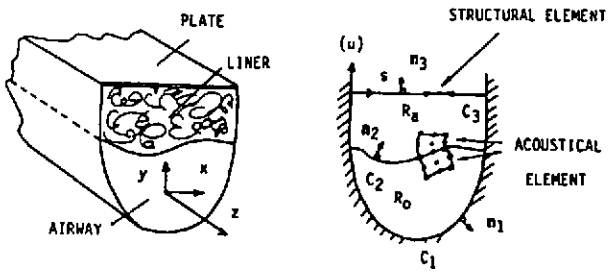

Figure 1. Geometry of the duct and its cross section.

These represent coupled structural/acoustic modes propagating along the duct with the same (complex) axial wavenumber 'α'. Substitution of expressions (7) into equations (1) and (2) yields

$$\nabla^2 p' + (k^2 - \alpha^2)p' = 0 \quad \text{in } R_o \text{ and } R_a, \tag{1a}$$

and $$g(d^4u/ds^4 - 2\alpha^2\, d^4u/ds^4 + (\alpha^4 - k_p^4)u) = p, \text{ on } C_3, \tag{2a}$$

where '∇^2' is the 2-D Laplacian ($\partial^2/\partial x^2 + \partial^2/\partial y^2$) and where $k_p^4 = q\,\Omega^2/g$.

Boundary conditions (3)-(6) are unaltered provided that the superscripts ' are dropped from the variables 'p' and 'u' and provided that the gradient operator $\underline{\nabla}$ is re-interpreted in its two dimensional form as $(\partial p/\partial x, \partial p/\partial y)$. The above equations pose a non-linear, complex eigenvalue problem in 'α'.

2.3 The variational statement.
Equations (1a) and (2a) are 'Euler' equations for the functional

$$F(u,p'_o,p'_a) = \tfrac{1}{2}\rho_o\,\Omega^2 \int_{C_3}\{g(u_{ss}^2 + 2\alpha^2 u_s^2 + (\alpha^4 - k_p^4)u^2) - up_a\}ds +$$

$$\tfrac{1}{2}\int_{R_o}\{\underline{\nabla}p_o\cdot\underline{\nabla}p_o - (k_o^2 - \alpha^2)p_o^2\}dxdy + \tfrac{1}{2}(\rho_o/\rho_a)\int_{R_a}\{\underline{\nabla}p_a\cdot\underline{\nabla}p_a - (k_a^2 - \alpha^2)p_a^2\}dxdy. \tag{8}$$

They arise naturally from the variation of 'u' and 'p' respectively. Moreover, boundary conditions (3),(4), and (6) emerge from the same process as 'natural' boundary conditions associated with the variation of p, provided that p is not specified on C_1 or C_3 and provided also that the class of functions from which it is drawn explicitly satisfies boundary condition(5) (i.e $p_a = p_o$ on C_2). The 'natural' boundary conditions associated with the variation of 'u' then correspond to clamped or simple supports along the edges of the plate. The solution of the eigenvalue problem posed by equations (1a) and (2a) and by boundary conditions (3)-(6) therefore reduces to the location of the stationary values of functional F. This is achieved in an approximate form using a Rayleigh-Ritz approach with trial functions defined by an FE model for the duct and the plate.

2.4. The finite element model.
Trial functions are formed for 'p' and 'u' by dividing the duct and plate into discrete elements. In the present analysis, nine noded isoparametric Lagrangian elements are used for the duct and two noded Hermitian line elements for the plate (see figure 1b). The nodal values of acoustic pressure, $p_1, p_2, \ldots p_{na}$ say, then define the pressure field in the airway and the liner. The degrees of freedom of the structural representation are the nodal displacements and rotations (about the z axis) at each structural node. These are denoted by $d_1, d_2, \ldots d_{ns}$. The finite element discretisation may then be represented in matrix form as,

LINED DUCTS WITH FLEXIBLE WALLS

$$p=[N_1(x,y),.. N_{ns}(x,y)]\begin{bmatrix} p_1 \\ p_2 \\ . \\ p_{na} \end{bmatrix} = \mathbf{N}\,\mathbf{p}, \text{ and } u=[S_1(s),.. S_{ns}(s)]\begin{bmatrix} d_1 \\ d_2 \\ . \\ d_{ns} \end{bmatrix} = \mathbf{S}\,\mathbf{d}, \tag{9,10}$$

where $N_i(x,y)$ and $S_i(s)$ are the global shape functions of the acoustic and structural meshes. Substitution of (9) and (10) into expression (8) then approximates the functional F by an algebraic expression, F'say, where

$$F' = \tfrac{1}{2}[\,\mathbf{d}^T\mathbf{A}\,\mathbf{d} + \mathbf{d}^T\mathbf{B}\,\mathbf{p} + \mathbf{p}^T\mathbf{B}^T\mathbf{d} + \mathbf{p}^T\mathbf{C}\,\mathbf{p}\,] = [\mathbf{d}^T,\mathbf{p}^T]\begin{bmatrix}\mathbf{A} & \mathbf{B} \\ \mathbf{B}^T & \mathbf{C}\end{bmatrix}\begin{bmatrix}\mathbf{d} \\ \mathbf{p}\end{bmatrix} \tag{11}$$

and where

$$\mathbf{A} = \rho_o\,\omega^2 \int_{C_3}\{g(\mathbf{S}_{ss}^T\mathbf{S}_{ss} + 2\alpha^2\mathbf{S}_s^T\mathbf{S}_s + (\alpha^4-k_p^4)\mathbf{S}^T\mathbf{S})\}ds, \tag{12}$$

$$\mathbf{B} = \rho_o\,\omega^2 \int_{C_3}\{\mathbf{S}^T\mathbf{N}\}ds, \tag{13}$$

$$\mathbf{A} = \int_{R_o+R_a}(\rho_o/\rho)\{g(\mathbf{N}_x^T\mathbf{N}_x + \mathbf{N}_y^T\mathbf{N}_y + (\alpha^2-k^2)\mathbf{N}^T\mathbf{N})\}dxdy, \tag{14}$$

(where $\rho=\rho_a$, $k=k_a$ in R_a, and $\rho=\rho_o$, $k=k_o$ in R_o).

In terms of their dependence on 'α', the matrices **A**, **B** and **C** are of the form ; $\mathbf{A} = \mathbf{A0} + \alpha^2\,\mathbf{A2} + \alpha^4\,\mathbf{A4}$, $\mathbf{B} = \mathbf{B0}$ and $\mathbf{C} = \mathbf{C0} + \alpha^2\,\mathbf{C2}$, where **A0**, **A2**, ,... **C2** are constant. The stationary values of F' are then obtained by equating its derivatives, with respect to the components of **d** and **p**, to zero. This gives

$$\begin{bmatrix}\mathbf{A} & \mathbf{B} \\ \mathbf{B}^T & \mathbf{C}\end{bmatrix}\begin{bmatrix}\mathbf{d} \\ \mathbf{p}\end{bmatrix}=\begin{bmatrix}\mathbf{0} \\ \mathbf{0}\end{bmatrix}, \text{ or } \left[\begin{bmatrix}\mathbf{A0} & \mathbf{B0} \\ \mathbf{B0}^T & \mathbf{C0}\end{bmatrix}+\alpha^2\begin{bmatrix}\mathbf{A2} & \mathbf{0} \\ \mathbf{0} & \mathbf{C2}\end{bmatrix}+\alpha^4\begin{bmatrix}\mathbf{A4} & \mathbf{0} \\ \mathbf{0} & \mathbf{0}\end{bmatrix}\right]\begin{bmatrix}\mathbf{d} \\ \mathbf{p}\end{bmatrix}=\begin{bmatrix}\mathbf{0} \\ \mathbf{0}\end{bmatrix}, \tag{15}$$

which may be converted into a symmetric, linear eigenvalue problem in 'α^2' by factoring the matrix **A4** into lower and upper factors **L** and $\mathbf{L}^T$ and by introducing a new vector $\mathbf{d}'=\alpha^2\mathbf{L}^T\mathbf{d}$. Equation (15) then becomes

$$\left[\begin{bmatrix}-\mathbf{I} & \mathbf{0} & \mathbf{0} \\ \mathbf{0} & \mathbf{A0} & \mathbf{B0} \\ \mathbf{0} & \mathbf{B0}^T & \mathbf{C0}\end{bmatrix}+\alpha^2\begin{bmatrix}\mathbf{0} & \mathbf{L}^T & \mathbf{0} \\ \mathbf{L} & \mathbf{A2} & \mathbf{0} \\ \mathbf{0} & \mathbf{0} & \mathbf{C2}\end{bmatrix}\right]\begin{bmatrix}\mathbf{d}' \\ \mathbf{d} \\ \mathbf{p}\end{bmatrix}=\begin{bmatrix}\mathbf{0} \\ \mathbf{0} \\ \mathbf{0}\end{bmatrix}. \tag{16}$$

This produces 'na+2(ns)' coupled eigensolutions. The uncoupled structural and acoustical modes are obtained by removing the coupling matrix **B0** to give two independent eigenvalue problems:

(a) the uncoupled structural problem ('2(ns)'modes)

$$\left[\begin{bmatrix} -\mathbf{I} & \mathbf{0} \\ \mathbf{0} & \mathbf{A0} \end{bmatrix} + \alpha^2 \begin{bmatrix} \mathbf{0} & \mathbf{L}^T \\ \mathbf{L} & \mathbf{A2} \end{bmatrix}\right]\begin{bmatrix} \mathbf{d'} \\ \mathbf{d} \end{bmatrix} = \begin{bmatrix} \mathbf{0} \\ \mathbf{0} \end{bmatrix}. \qquad (17)$$

(b) the uncoupled acoustical problem ('na' modes)

$$[\ \mathbf{C0} + \alpha^2\ \mathbf{C2}]\mathbf{p} = \mathbf{0} \qquad (18)$$

2.5 Modal representation of a rigid/flexible transition.
Consider now the sound field in the vicinity of an abrupt transition from a rigid walled duct, in the region z<0 say, to a flexible walled duct, in the region z>0. The incident sound field in the rigid walled duct is known and the flexible walled segment is anechoic. The eigenmodes produced from the solution of equations (16) and (18) can readily be combined to produce a complete solution for the sound field on either side of the discontinuity.

Let the eigenvalues, pressure eigenvectors and structural eigenvectors produced by the solution of the coupled problem (equation (16)) be denoted by α^2_i, $\mathbf{p}_i$ and $\mathbf{d}_i$ respectively (i=1,nt where nt=na+2(ns)). The analogous modes for problem (18), that is, for the same duct but with rigid walls, are denoted by α'^2_j and $\mathbf{p'}_j$ say (j=1,na). In both cases the eigenvalues , α_i and α'_i, are chosen with negative complex parts and correspond to 'positive' modes, in the sense that they attenuate in the positive z direction. The sound field in the region, z<0, may then be written as a superposition of positively and negatively propagating modes in the rigid walled duct, that is, the acoustic pressure p'(**x**) may be written

$$p'(\mathbf{x}) = \sum_{n=1}^{na} \mathbf{N} \{a_n^+\ \mathbf{p'}_n \exp(-i\alpha'_n z) + a_n^-\ \mathbf{p'}_n \exp(+i\alpha'_n z)\}, \qquad (19)$$

where the incident coefficients, a_n^+, are known and the reflected coefficients a_n^- are to be determined. Similarly, the acoustic pressure and structural displacement in the region, z>0, are given by

$$p'(\mathbf{x}) = \sum_{n=1}^{nt} \mathbf{N} \{b_n^+ \mathbf{p}_n \exp(-i\alpha_n z)\} \text{ and } u'(z,s) = \sum_{n=1}^{nt} \mathbf{S} \{b_n^+\ \mathbf{d}_n \exp(-i\alpha_n z), \qquad (20)$$

where the transmission coefficients, b_n^+, are unknown. Acoustic pressure and normal particle velocity may then be matched across the plane z=0 . This may be done using point collocation (since the transverse mesh is identical in both regions) and produces 2(na) linear equations for the (na + nt) unknown coefficients (a_i^-, i=1,..na, and b_j^+ j=1,...nt). To complete the equations, it is necessary to specify the way in which the plate is secured at z=0. In the present instance, it is clamped and the displacement field given by expression (25) is constrained so that 'u' and $\partial u/\partial z'$ are zero at z=0. This yields the

'2(ns)' additional equations required for the determination of the unknown coefficients. These may then be substituted back into expressions (20) and (21) to give the sound field in the duct.

3. MEASUREMENTS

Figure 2 shows the experimental arrangement. A loudspeaker, fed with a sinusoidal signal or white noise, radiated into a rigid-walled section of rectangular lined duct, followed by a lined duct section with three rigid walls and one flexible wall, rigidly clamped along its sides and where it joined the fully rigid section. At the far end of the duct, a sound-absorbing termination largely eliminated acoustic reflections, and wedges of structural damping material attached to the flexible wall reduced structural wave reflections. The acoustic absorbent was a fully reticulated polyurethane foam 30 mm thick, with a steady viscous flow resistivity of 6230 SI rayls/m. Its bulk acoustic properties were measured in separate tests by using an impedance tube. The flexible wall was of aluminium, 0.54 mm thick and 100 mm wide; the absorbent was placed next to the flexible wall, with a very small air-gap between the two. Sound pressure data were taken at a series of axial pressure tapping and vibrational data were taken along the wall. Because the metal bars used to clamp the flexible wall had a small degree of transverse curvature to their notionally flat sides, the wall was actually clamped a small distance from the corners of the bars, and the effective width of this wall was 107 mm.

4. COMPARISON BETWEEN NUMERICAL AND MEASURED DATA.

Figures 3 and 4 show the real and imaginary parts of the computed axial wavenumber, as a function of frequency (the imaginary part has been converted into an attenuation per unit length), for the least attenuated modes in the test duct. Also shown are the exact (see [1]) corresponding values for a lined, but rigid-walled, duct. The (real) axial wavenumber of the first uncoupled structural mode (see [5]) is also shown.

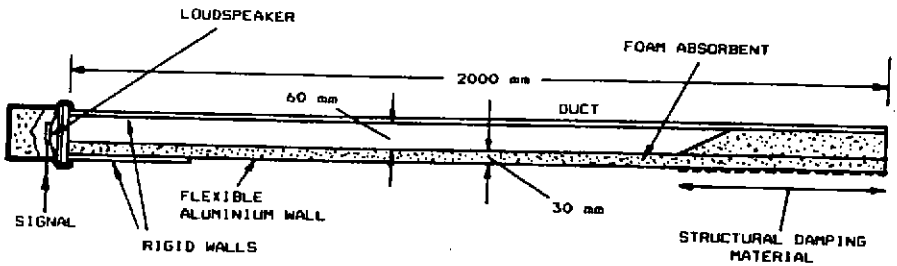

Figure 2. Experimental duct.

LINED DUCTS WITH FLEXIBLE WALLS

Although not shown, the FE values for the uncoupled acoustical and structural wavenumbers (obtained from the solution of equations (17) and (18)) could not be distinguished, to the scale of Figures 3 and 4, from their 'exact' counterparts.

At all frequencies there is one coupled mode corresponding to the least attenuated rigid-duct mode, but this alternates between modes I, II and III. This role changes from I to II through the first structural resonance (at 260 Hz), from II to III through the second resonance, and so on. Coupling occurs at these frequencies between modes which are predominantly 'structural' and those which are predominantly 'acoustical', and appears to be the mechanism for the attenuative peak at the first resonance. Its presence is supported by the experimental data in Figure 5, where the measured attenuation beyond the rigid/flexible wall transition and values computed from the modal solution of Section 2.5 are compared. Two sets of measured data are shown: those based on the average slope of the axial sound level, and those measured directly as the difference between values at the transition and a point 1 m beyond it.

Figure 6 shows the axial wall displacement on the centreline at 300 Hz. Correspondence between measured and computed values is good. Both clearly demonstrate the presence of significant modal mixing.

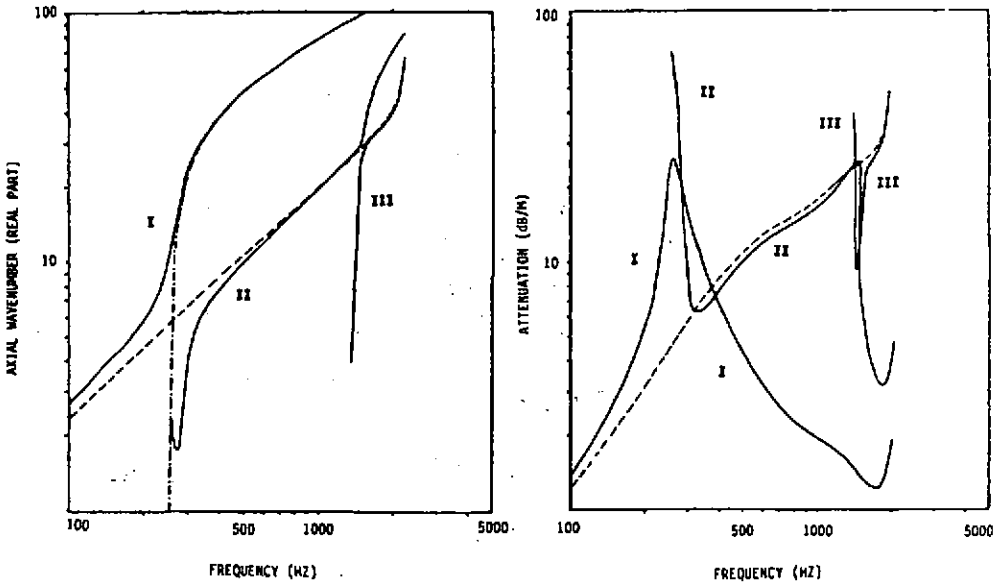

Figure 3,4,: axial wavenumber (real part) and axial attenuation, test duct.
—— FE soln.,–– exact(lined,rigid),–·– exact(1st struct.mode).

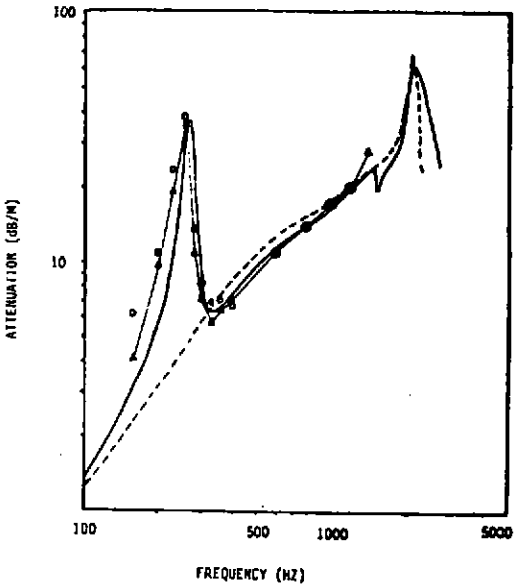

Figure 5: Effective attenuation; — FE, ○ measured -▲- measured (averaged).

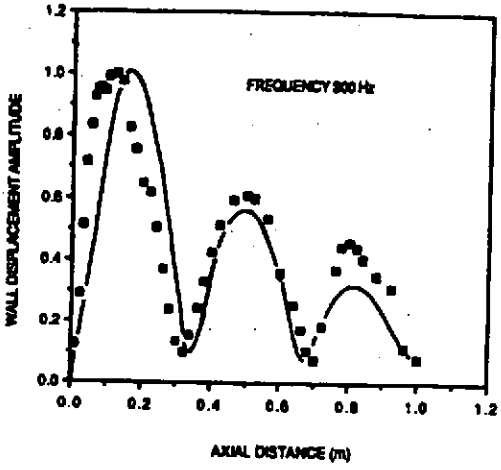

Figure 6: Wall displacement; — FE, ⊡ measured.

5.CONCLUSIONS

Comparisons of measured and computed results indicate that the effects of wall flexibility on sound transmission in bulk lined ducts are accurately modelled using an FE formulation, and that these effects are significant in the vicinity of structural resonances. The coupling between 'structural' and 'acoustical' modes is then quite strong and produces unexpected results, particularly in regard to attenuation, when compared with the acoustical field in an equivalent duct with rigid walls.

6.ACKNOWLEDGEMENTS

The authors wish to acknowledge support from the S.E.R.C. under research grants GR/F/59407 and GR/F/56819 and from Sound Attenuators Ltd. of Colchester.

7.REFERENCES

[1] R.A. SCOTT Proceedings of the Physical Society 58, 358-368 (1946).
[2] C.WASSILIEFF Journal of Sound and Vibration 114,239-251(1987)
[3] R.J.ASTLEY and A.CUMMINGS Journal of Sound and Vibration 116 239-263.(1987)
[4] A.CUMMINGS Journal of Sound and Vibration 61 327-345 (1978).
[5] A.CUMMINGS Journal of Sound and Vibration 74 351-380 (1981).

Proceedings of the Institute of Acoustics

ACOUSTICS OF CONICAL DIFFUSERS

P O A L Davies

Institute of Sound and Vibration Research, Southampton University, Southampton, SO9 5NH

1. INTRODUCTION

Conical pipes connecting two pipes of constant but differing diameter often form elements of acoustically excited flow ducts. Normally, excitation frequencies remain sufficiently low so that the transverse dimensions of all pipes remain a small fraction, with the lengths of conical pipes a modest fraction, of the acoustic wavelength. One can then assume that the wavefronts of the sound propagating in the uniform pipes remains effectively plane, while the wavefront shapes in the conical pipes will be spherical. It is convenient to subdivide such elements into two further classes. One such may be treated as sufficiently short that both the hydrodynamic and acoustic behaviour corresponds closely to that for an abrupt expansion or contraction in area. This case can then be modelled approximately, but perhaps realistically in practice, by adopting the analytical methods describing wave propagation across sudden area charges outlined, for example, in reference [1]. Here appropriate allowance has been included for flow separations at the corners with the consequent flow and acoustic losses that occur. Normally, flow contractions can be short without incurring undue losses, but this is not generally true with expansions.

The other class, which forms the subject of this contribution, includes those examples of expanding flows where the axial rate of area change is sufficiently small that flow separation is avoided. (What follows is also applicable to long gently contracting nozzles, which are relatively less commonly found). With this restriction the flow can be regarded as homentropic and irrotational so that the relevant and recent theoretical analysis of the acoustic behaviour, presented in references [1] and [2], is then appropriate. An outline of the discussion given there is repeated here, with some relevant experimental observations.

1.1 Geometrical features

The geometry concerned is illustrated in figure 1, showing a cone of axial length l with taper angle α connecting a smaller pipe, diameter $2a_0$, where the mean flow Mach number is M_0, to a larger one, diameter $2a_1$. Transfer between the plane wave motion in the pipes and the spherical wave motion in the cones is assumed to occur within the lens shaped control volume V_r shown hatched. This is bounded by a plane surface of area S_p and a spherical cap of area S_s. From the geometry $\alpha = \arctan[(a_1-a_0)/l]$ with radial distance from the apex $r = a_r \mathrm{cosec}\alpha$. Also $S_p = \pi r^2 \sin^2\alpha$, $S_s = 2\pi r^2 (1-\cos\alpha)$ and $V_r = (\pi/3)\, r^3 (1-\cos\alpha)^2 (2+\cos\alpha)$. The maximum limit, implied by the requirement that the mean flow remains attached at the cone walls, suggests $\alpha < 0.1$ radian or thereabouts. With $\alpha = 0.1$ radian the ratio $S_s/S_p = 1.0025$, so that both S_s and S_p will be taken here, for convenience, as equal to their arithmetic average $S_r = (S_p + S_s)/2$.

ACOUSTICS OF CONICAL DIFFUSERS

In the applications considered here r is of order unity or less in terms of acoustic wavelengths, so that V_r is a relatively small volume with thickness $r(1 - \cos \alpha) < 0.01$ in the same relative terms. Within each volume V_r, mass will be conserved, the associated mass flux being those on the outward normal directions on S_s and S_p and momentum will be similarly conserved. The fluctuating mass of the fluid within the control volume is involved in both the mass and momentum balances, in effect providing an end correction at the junction. Within V_r the fluctuating motion associated with wave transfers at the ends of the cone is neither quite plane or quite spherical. However, a permissible simple but balanced and quite accurate approximation is to assume that each fluctuating quantity in V_r is the arithmetic average of its plane S_p-side and spherical S_s-side representations. With this approximation, the representative average thickness of the volume of fluctuating mass associated with the two bounding surfaces S_p and S_s will be expressed by $T_r = (1/2)\, V_r/S_r$.

2.1 Wave motion in the cone

With modest values of the mean flow Mach number $M_o < 0.2$, it can be readily demonstrated [2] that the flow temperature remains constant to better than 0.8%, implying that the speed of sound c in the cone can be assumed a constant c_o to better than 0.4%. The approximate analytic solution developed in [2] assumes purely radial flow in the cone so that the mean velocity is proportional to $(r_o/r)^2$ and the Mach number at any r, $M_r = (r_o/r)^2\, M_o$. The pressure, p, mass density, ρ, and particle velocity, u, in the cone are functions of r and time t, while the corresponding variables in the pipes are functions of the axial position x and time t. One can express all these variables as the sums of mean and fluctuating quantities, the latter having zero time averages. Thus $p(r,t)$ can be expressed as $\overline{p}(r) + p'(r,t)$, and so on for the others. For potential flow, with $\phi(\rho,t) = \overline{\phi}(r) + \phi'(r,t)$ one has $u(r,t) = -\partial \overline{\phi}/\partial r - \partial\phi'(r,t)/\partial r$. As there is only one space co-ordinate involved as an independent variable, the velocity is irrotational. For simplicity the flow is assumed to be homentropic.

Conservation of mass can then be expressed by

$$(1/c^2)\, Dh/Dt - \nabla^2\phi = 0 \qquad (1)$$

where $c^2 = \gamma p/\rho$, γ the ratio of the specific heats, h the enthalpy per unit mass and D/Dt is the material derivative. With homentropic irrotational flow the expression for conservation of momentum can be integrated to give a conservation of energy expression

$$h + (1/2)\,(\nabla\phi)^2 - \partial\phi/\partial t) = h_o \qquad (2)$$

where h_o is a constant reference enthalpy. With an ideal gas where $h = c^2/(\gamma-1)$ it is shown in [2] that with Mach numbers $|\nabla\phi/c_o|$ less that 0.2, c^2 can be regarded as a constant in equation (2). With spherical polar coordinates and purely radial flow, substitution for h from equation (2) into equation (1) gives ultimately, [2],

$$[c^2 - (\partial\phi/\partial r)^2]\,\partial^2\phi/\partial r^2 + 2[(c^2/r) + (\partial\phi/\partial r)\,\partial/\partial t]\,\partial\phi/\partial r - \partial^2\phi/\partial t^2 = 0 \qquad (3)$$

which must be satisfied by both mean and fluctuating components of the velocity potential ϕ.

For the mean motion, for $M_o < 0.2$, after time averaging (3), it is shown [2] that the resulting equation describing the mean motion is satisfied to better than ± 4% at least by the velocity potential $\overline{\phi} = -u_o r_o^2/r$, which being proportional to r, satisfies Laplace's equation in $r_o \le r \le r_1$. It is also shown that equation (3) then reduces to

$$c_o^2\,\partial^2\phi'/\partial r^2 + 2[c_o^2/r - u_o\,(r_o/r)^2\,\partial/\partial t]\,\partial\phi'/\partial r - \partial^2\phi'/\partial t^2 = 0 \qquad (4)$$

which is linear in $\phi'(r,t)$, with coefficients that are only functions of r.

An appropriate compact solution to equation (4) expressed in terms of ϕ^+ for waves travelling in the positive r direction and ϕ^- for those travelling in the converse was then found [2] to be

$$\phi^+ = (G_o^+/r)\exp[i\,(\omega t - k_s^+ r)], \qquad k_s^+ = (\omega/c_o)\,(1+M_r), \qquad (5a)$$

$$\phi^- = (G_o^-/r)\exp[i\,(\omega t - k_s^- r)], \qquad k_s^- = (\omega/c_o)\,(1-M_r), \qquad (5b)$$

with $M_r = (r_o/r)^2\,M_o$, which is again accurate to better than ±4% with $M_o < 0.2$. Fluctuating velocities and pressures in the conical pipe can then be found in the normal way from

$$u' = -\partial\phi'/\partial r, \qquad p' = \rho\,(\partial/\partial t + \overline{u}\,\partial/\partial r)\,\phi', \qquad (6,7)$$

where ρ can be assumed constant [2,3] and equal to ρ_o and $\overline{u} = u_o\,(r_o/r)^2$.

2.2 Wave transfer at the cone/pipe junctions

Conservation of mass and momentum in the junction control volume V_r, respectively, can be concisely expressed in Cartesian tensor notation (i, j = 1,2,3), as

$$\int_{V_r} \frac{\partial \rho_{vr}}{\partial t}\,\partial V_r + \int_{S_s} \rho_s u_s\,\partial S_s + \int_{S_p} \rho_p u_p\,\partial S_p = 0 \qquad (8)$$

$$\int_{V_r} \frac{\partial}{\partial t}(\rho u_i)_{vr}\,\partial V_r + \int_{S_s} (\rho_s u_{si} u_{sj} + p\delta_{ij})\,dS_{sj} + \int_{S_p} (\rho_p u_{pi} u_{pj} + p_p \delta_{ij})\,dS_{pj} = 0. \qquad (9)$$

(Here δ_{ij} is the Kronicker delta, equal to unity for i=j and zero for i≠j). With the variables written as sums of mean and fluctuating parts, with the latter assumed small so their squares can be neglected, each of equations (8) and (9) can be separated into independent time averaged and fluctuating parts. It can then be shown [3] with the temperature assumed constant within ±0.8% or better are also corresponding constant c_o throughout the system, it is consistant to assume that the mean pressure and density are also constant everywhere in the cone.

The fluctuations, being governed by linear equations can conveniently be expressed in term of the Fourier coefficients of the fluctuating particle velocities and pressures of the component waves. Thus, with plane waves of frequency ω, (See reference [1]) one can adopt the well established substitutions

$$p_p' = p_p^+ + p_p^- = p_p^+(o) \exp i(\omega t - k_p^+ x) + p_p^-(o) \exp i(\omega t + k_p^- x), \qquad (10)$$

where $k_p^+ = k/(1+M_r)$, $k_p^- = k/(1-M_r)$ and $k = \omega/c_o$. Also $p_p^+(o)$ corresponds to the amplitude of the positively travelling waves at the origin for x. For fluctuating particle velocities, the corresponding isentropic substitution [1] is

$$\rho_o c_o u'_p = p_p^+ - p_p^-. \qquad (11)$$

The corresponding fluctuating quantities in the cone, at frequency ω, are

$$u_s' = u_s^+ + u_s^- = [(1/r) + ik(1-M_r)]\,\phi_s^+ + [(1/r) - ik(1+M_r)]\,\phi_s^-, \qquad (12)$$

$$p'_s = \rho_o c_o [\{ik - M_r[(1/r) + ik_s^-]\}\,\phi_s^+ + \{ik - M_r[(1/r) - ik_s^+]\}\,\phi_s^-]. \qquad (13)$$

Following the discussion concerning the averaged motion in V_r, at the end of section 1.1, one finds for example $\int_{V_r} (\partial\rho_{vr}/\partial t)\, dV_r$ in equation (8) becomes simply $(1/2)(\partial\rho_s/\partial t + \partial\rho_p/\partial t)\, V_r$ and similarly for the volume integral in (9). Thus the fluctuating part of the mass balance equation (8) can be written with $\overline{u}_s = \overline{u}_p = c_o M_r$, as

$$(1/2)\, i\omega V_r (\rho_s' + \rho_p') = S_r(\rho_o u_s' + c_o M_r \rho_s') - S_r(\rho_o u_p' + c_o M_r \rho_p') = 0 \qquad (14a)$$

with $T_r = (1/2)\, V_r/S_r$ and the isentropic substitution $\rho' = p'/c_o^2$, rearranging, collecting terms and multiplying through by c_o converts this equation to the more convenient form

$$(M_r + ikTr)\, p'_s + \rho_o c_o u_s' = (M_r - ikTr)\, p'_p + \rho_o c_o u'_p. \qquad (14)$$

Similarly, the fluctuating part of the momentum balance (9) can be expressed as

$$(1 + M_r^2 + ikM_rT_r)\, p_s' + \rho_o c_o\, (2M_r + ikT_r)\, u_s' = (1 + M_r^2 - ikM_rT_r)\, p'_p + \rho_o c_o\, (2M_r - ikT_r)\, u_p'. \quad (15)$$

when p' and u' in equations (14) and (15) are expressed via equations (10) to (13), in terms of $\phi_s^{\pm}$ and $p_p^{\pm}$, then given either one pair they can be solved to determine the other. To avoid tedious algebra, equation (15) can be simplified at the outset [3] be neglecting the terms M_r^2 and $k\, M_rT_r$ compared with unity and approximated by

$$p_s' + \rho_o c_o\, (2M_r + ikT_r)\, u_s' = p_p' + \rho_o c_o\, (2M_r - ikT_r)\, u'_p. \quad (15a)$$

With similar simplifications, use of equations (10) to (13) with M_r^2 terms neglected) in equations (14) and (15a) gives, after again neglecting terms which arise in M_r^2 and kM_rT_r in comparison with unity, for the approximate mass balance,

$$\rho_o c_o\, [\{(1/r) - k^2T_r\}\, (\phi_s^+ + \phi_s^-) + ik\, (\phi_s^+ - \phi_s^-)] = (M_r - ikT_r)\, (p_p^+ + p_p^-) + (p_p^+ - p_p^-), \quad (16)$$

and for the corresponding momentum balance

$$\rho_o c_o\, [\{(1/r)\, (M_r + ikT_r) + ik\}\, (\phi_s^+ + \phi_s^-) + ik(M_r + ikT_r)\, (\phi_s^+ - \phi_s^-)]$$

$$= (p_p^+ + p_p^-) + (2M_r - ikT_r)\, (p_p^+ - p_p^-). \quad (17)$$

Wave transfers across the junctions between pipe and cone or cone and pipe can be calculated by solving equations (16) and (17). Wave transfer along the cone can be calculated from equations (5a) and (5b). This completes the theoretical analysis. It now remains to compare the predictions with observations.

3.1 Experimental procedures

A general model of an acoustic system is illustrated in figure (2a). Here, the element of interest (eg the cone) is represented by its scattering matrix [T], see ref [1], and lies between its source of excitation S and an acoustic load with impedance Z. The four complex wave amplitudes $p_1^{\pm}$ and $p_2^{\pm}$ yield four ratios which describe its in-situ acoustic characteristics. these are the two transmission coefficients, defined by

$$Ti = p_1^+/p_2^+, \qquad Tr = p_1^-/p_2^- \quad (18), (19)$$

with reflexion coefficients

$$r_1 = p_1^-/p_1^+, \qquad r_2 = p_2^-/p_2^+ \quad (20), (21)$$

One notes that any 3 of the 4 serve to define all 4. Furthermore, if Z is known, the $r_2 = (Z-\rho c) / (Z+\rho c)$, so that any two others then suffice. In such cases, it is sufficient to measure, or calculate say, Ti and r_1.

The pair of wave component amplitudes $p^{\pm}$ and hence r_1 and r_2 can be measured independently by the now well known two transducer method described, for example, in reference [4] and employed successfully be the author and his associates at Southampton for the past 15 years or so. However similar estimates of Ti an Tr require a four transducer method, as described in references [5, 6] with the experimental arrangement illustrated in figure (2b). Assuming plane wave propagation and uniform mean flow, each of the complex amplitudes of the monochromatic components Pn of the observed signals at stations 1, 2, 3, 4 is the sum of corresponding component wave contributions P_n^+ and P_n^-. Thus $P_1 = P_1^+(o) \exp(-i\beta^+ x_1) + P_1^-(o) \exp(i\beta x_1)$, where $\beta^{\pm}$ is the corresponding complex wave number [4] accounting both for mean flow and wave attenuation, while $P_1^{\pm}(o)$ are the component wave amplitudes at the correspoding origin for x. With white noise excitation simultaneous records of the four pressures can be expressed in matrix form: $\mathbf{P} = \mathbf{K}.\mathbf{Po}$, where the vector **P** contains their Fourier transforms, **Po** contains the complex wave component amplitudes $P^{\pm}(o)$ and the matrix **K** is composed of the corresponding exponential terms.

Assuming the random pressure field in the system is stationary and ergodic, the spectral density functions between two signals at stations m and n can be expressed as Smn(f). A spectral matrix which contains all the auto and cross-spectral densities Smn can then be built

$$S_p(f) = \{\mathbf{P}^*(f).\ \mathbf{P}^T(f)\} = \mathbf{K}^*.\ \mathbf{S}(o).\ \mathbf{K}^T, \qquad (22)$$

where the operator { } represents an ensemble average an the star denotes the conjugate. The matrix $S(o) = \{P_o^*(f).\ P_o^T(f)\}$ of the spectral densities of the component waves can be estimated by inverting (22),

$$S(o) = K^{*-1}.\ Sp.\ K^{-T}$$

The reflexion and transmission coefficients are estimated as transfer functions of a single input linear system, with the less noisy upstream signals chosen for the inputs. Further details can be fond in references [5, 6].

3.2 Comparison of measurements with predictions

Observations of Ti and r_1 were made with a conical diffuser 0.24m long where $2a_0 = 38$mm and $2a_1 = 71$ mm, giving $\alpha \sim 0.07$ radian, with mean flow Mach numbers ranging from zero to 0.2. The tailpipe of diameter $2a_1$, attached to the cone outlet, was 1.0m long, its acoustic impedance representing the load Z in figure (2a). The signal was excited with white noise at a level well above background noise over the frequency range of interest and the spectral density functions were calculated from signal records 10 sec along with an averaging bandwidth of 10 Hz yielding estimates with some 400 statistical degrees of freedom.

Preliminary results of measurements of Ti and r_1 indicate that a close agreement exists between them and predictions calculated with the analytical relations set out in section 2. More comprehensive comparisons will be reported in due course.

References

[1] P O A L Davies, 'Practical Flow Duct Acoustics', J Sound and Vibration 124, 91-115 (1988)

[2] P O A L Davies, and P E Doak 'Spherical Wave Propagation in a Conical Pipe with Mean Flow', J Sound and Vibration 137(2), 343-346 (1990)

[3] P O A L Davies and P E Doak 'Wave Transfer to and from Conical Diffusers with Mean Flow', J Sound and Vibration 138 (in press) (1990)

[4] P O A L Davies, M Bhattacharya and J E Bento Coelho 'Measurement of Plane Wave Acoustics Fields in Flow Ducts' J Sound and Vibration 72, 539-542, (1980)

[5] J L Bento Coelho, 'Techniques for Efficient Measurement of Flow Duct Element Acoustic Characteristics,' Internoise 84, 429-432, (1984)

[6] J L Bento Coelho, 'Acoustic Characteristics of Perforate Liners in Expansion Chambers', PhD Thesis, University of Southampton (1983)

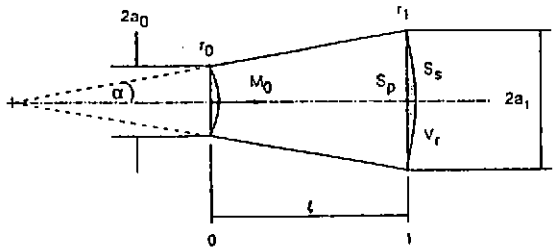

Figure 1

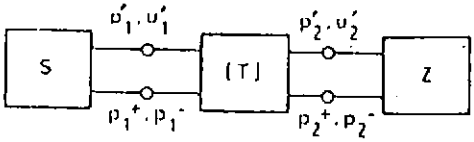

Figure 2a

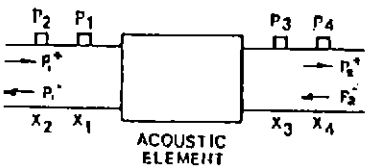

Figure 2b

Proceedings of the Institute of Acoustics

A MODEL OF FINITE AMPLITUDE SOUND PROPAGATION IN HORNS

K R Holland & C L Morfey

ISVR University of Southampton

1. INTRODUCTION

The high electro-acoustic efficiency of horn/compression driver loudspeaker systems leads to their use for the production of high sound pressure levels. In order to produce high levels in the far field, very large acoustic pressures must be present at the small throat of the horn and especially in the phase plugs of the drivers. A high quality compression driver typically has a sensitivity of 143dB SPL into a plane wave tube for 1W of electrical power input. The same driver may have a thermally limited maximum power capability of 100W leading (assuming linearity) to acoustic pressures in excess of 160dB SPL at the throat of a horn. When the typically 20:1 compression ratio for the driver is considered, acoustic pressures in excess of 180dB SPL are possible at the diaphragm. It is clear from the above maximum levels that linear acoustic modelling of the horn and driver will not be accurate at high drive levels.

Of the many sources of system nonlinearity possible at these levels, three are expected to be predominant. One involves the electro-mechanical limitations of the driver, including thermal power compression effects, magnet/gap problems etc. The second source of nonlinearity involves the volumetric changes in the cavity between the diaphragm and the phase plug, and the third, with which this model is concerned, involves propagation nonlinearity leading to the possibility of the production of shock waves in horns and drivers. Whereas the fist nonlinear mechanism is common to all electro-magnetic loudspeakers, the second and third mechanisms are peculiar to horns in that they are acoustic nonlinearities.

2. DESCRIPTION OF MODEL

If it could safely be assumed that the sound field within horns and that radiated to the far field consisted of a single progressive wave from throat out to infinity, the calculation of the sound field, to reasonable accuracy, for finite amplitudes would not be too difficult. However, all practically realisable horns suffer reflections from the mouth termination and often from discontinuities within the horn flare. This being the case, it is impossible to follow the propagation of a wave from the throat to the mouth and back again as is possible for infinitesimal amplitude (linear) modelling because linear superposition does not apply and the forward and backward waves will interact in an unknown manner. It is therefore necessary to model the system "backwards" in time from the far field, where linearity is assumed, to the throat. In the model described below, nonlinear propagation has been modelled in this manner initially by investigating what input waveform would be necessary to produce a sinusoidal output in the far field (a form of pre-distortion).

In order to model horns of arbitrary shape it is necessary to split the horn into short exponential

elements. However, because the interaction between the forward and backward waves is likely to vary within the space of one wavelength, the model may require many elements of length not greater than a fraction of a wavelength of the highest frequency of interest (possibly including harmonics).

The speed of propagation of a sound wave at a point is dependent upon the local pressure and particle velocity at that point. In a free, progressive wave this results in the positive half cycle of a waveform propagating faster than the negative half cycle giving rise to steepening of sinusoids and eventual shock formation. Under most conditions at moderate levels, dissipative mechanisms in the sound medium and the large propagation distances involved prevent this from being significant, and linearity can safely be assumed. The situation within horns at high levels is not this simple. The characteristic impedance of a wave within a horn is usually complex due to phase dispersion and reflections, so the equations used for the calculation of waveform steepening in free, progressive waves cannot be used. Instead a more universal equation for the local propagation speed (c(t)) is used:

$$c(t) = c_0 \left\{ \frac{P_0 + p(t)}{P_0} \right\}^{\frac{\gamma-1}{2\gamma}} \pm u(t) \quad , \tag{1}$$

where c_0 is the linear assumed sound speed for the particular static pressure (P_0), p(t) and u(t) are the instantaneous total (forward & backward waves) acoustic pressure and particle velocity respectively, γ is the ratio of the specific heats of the sound medium and $\pm$ refers to calculation for forward and backward waves respectively. The "time advance" (T) of a portion of a waveform compared to its linear propagation can then be calculated:

$$T(t) = -l \left\{ \frac{1}{c(t)} - \frac{1}{c_0} \right\} \quad , \tag{2}$$

where $-l$ is the distance propagated. The concept of a negative propagation distance is introduced to avoid the complications involved with negative time and hence negative velocities. These propagation speed calculations can only be carried out in the time domain, where calculation of the dispersive and reflective properties of a horn are difficult. To overcome this problem, calculations are carried out both in the time domain and in the frequency domain and linked via 256 point Fast Fourier Transforms. The following is a description of the model, a flow diagram is shown in fig.1.

A starting waveform ($p_0(t)$) is defined as the desired output, along with the coordinates of the horn and the output impedance ($Z_0(f)$). The output pressure waveform is transformed into the frequency domain (p(f)) and a closed form linear solution of Webster's Horn Equation [1], uses the horn coordinates and the output impedance to separate out the forward and backward pressures and particle velocities ($p_A(f)$,$p_B(f)$,$u_A(f)$ & $u_B(f)$ resp.) and propagate them back to the end of the element. The two pressures are transformed into the time domain and added ($p_T(t)$) as are the particle velocities ($u_T(t)$). These total waveforms are used to calculate the propagation speeds ($c_A(t)$ & $c_B(t)$) for every time point using equation (1) which along with the horn coordinates (to obtain the element lengths) are used to calculate the time advances for every time point. These time advances are checked at this point to ensure that none of the time

points "overlap" indicating shock generation. If shocks are detected, the programme stops and announces the presence of a shock (the model cannot as yet handle shock propagation). Each of the four separate time waveforms ($p_A(t)$,$p_B(t)$,$u_A(t)$ & $u_B(t)$) are distorted using the time advances and resampled to maintain linear time spacing for FFT calculations. The two distorted pressure waveforms are then added and transformed back into the frequency domain and fed back to the start of the next element ($p(f)$). The particle velocity waveforms are also added and transformed and used in conjunction with the total pressure to calculate the impedance for the new element ($Z(f)$). The process is repeated for each element in turn until the throat of the horn is reached or a shock is generated. The end waveform can then be considered to be that input necessary to obtain the starting waveform ($p_o(t)$) as an output.

The model as described appeared to work well but when tested with an increasing number of elements, it was found that more elements were required than expected before the result converged. If enough elements were not used, the model tended to overestimate the nonlinearity compared to the result for a large number of elements. This problem was traced to the fact that the total pressure and particle velocity values that were used for the speed of propagation calculations were those that occured at the end (throat) of each element and as such the calculations were always the "worst case" approximations to the actual nonlinearity. To overcome this problem a weighting function (shown dotted) was introduced into the calculations assuming that, for a given forward or backward wave, the product of the pressure and the square root of the area remained constant throughout an element. Because of the exponential shape of each element, the integral of this function over an element appears as a multiplying constant in both the pressure and particle velocity terms. The only other assumption inherent in this is that the "distorting effect" varies linearly with pressure and particle velocity over an element, this is reasonable for a short element. After this modification, convergence was seen to be very much better and reliable results could be obtained with fewer elements.

Another problem became apparent only when a large number of elements were used ($n>20$) and the starting waveform was a sinusoid. It is reasonable to assume that any distortion should appear only as harmonics of the continuous starting sinusoid, however when such a starting waveform was used, after propagation through a large number of elements, spurious frequencies were observed on the spectra. This was traced to the lack of any signal at those frequencies allowing the errors (noise) in the computations to appear as very large numbers in the calculation of impedance at those frquencies (a small number divided by a very small number giving a large number) which after a large number of elements allowed significant values for pressure to appear. A first attempt to overcome this problem was to "pad" the starting waveform with a small delta function to give some signal at all frequencies. This resulted in the gross amplification at low frequencies below the cut-off of the horn (where large amounts of "input" were necessary at the throat to appear as small outputs on the starting waveform) making the problem worse. Finally it was decided that for sinusoidal starting waveforms, only the harmonics would be calculated in the frequency domain, all other frequencies being held to zero. This technique appears to work well. For transient starting waveforms the problem does not occur.

Fig. 2 shows a sinusoidal starting waveform at the mouth of a typical midrange horn. Figs. 3, 4 & 5 show the throat waveform results for three different frequency starting waveforms. The starting pressure and normalised impedance are 140dB and 1 respectively at the horn mouth.

3. PROPOSED FUTURE DEVELOPEMENT

Although within the horn itself boundary absorption and dispersion effects may not significantly effect results, if the model is to extend back to the diaphragm through the phase plug where dimensions can be of the order of fractions of a millimeter, these effects must be included. It is proposed to extend the model to include these effects, along with flow resistive and turbulent phenomena. If this can be achieved, the model should prove a very powerful tool in the analysis of finite amplitude standing wave fields in waveguides. The absolute accuracy of the model is difficult, if not impossible to check because of the many sources of nonlinearity in the chain. This problem apart, it may be possible to drive a horn with the output waveform from the model using an extremely linear driver and see if the output becomes sinusoidal as level is increased. At worst, calculated values for harmonic distortion could be compared to measurements. Tests of this kind as well as more general harmonic distortion measurements are planned.

4. REFERENCES

[1] A G WEBSTER, "Acoustical Impedance and the Theory of Horns and of the Phonograph", Proc. Natl. Acad. Sci. (U.S.) 5, pp 275-282, (1919).

FINITE AMPLITUDE HORN PROPAGATION

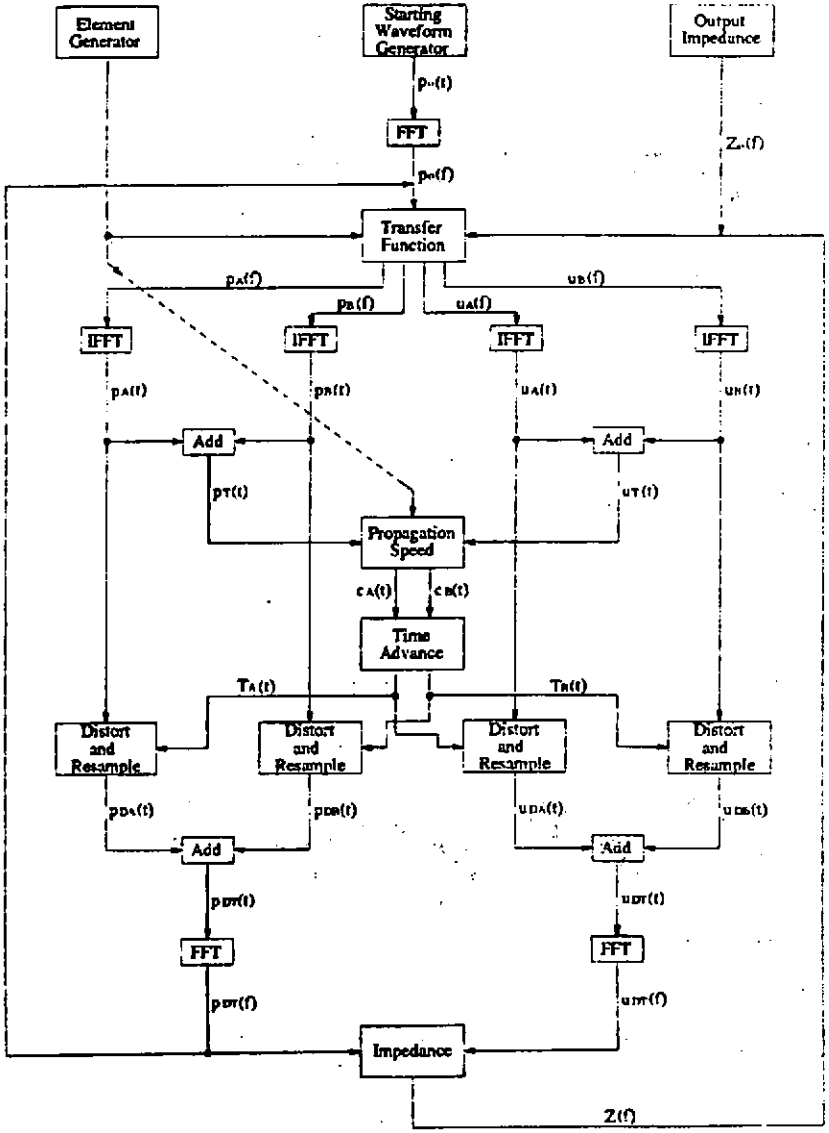

Fig. 1 Flow Chart for Finite Amplitude Horn Model.

FINITE AMPLITUDE HORN PROPAGATION

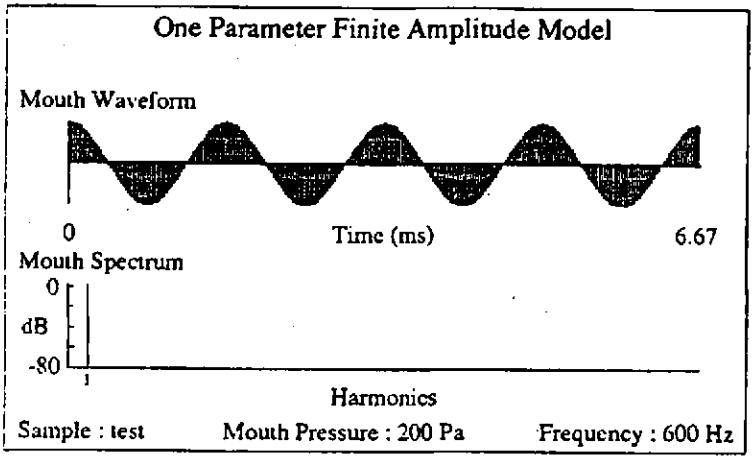

Fig. 2 600 Hz Mouth Starting Waveform and Spectrum (model input).

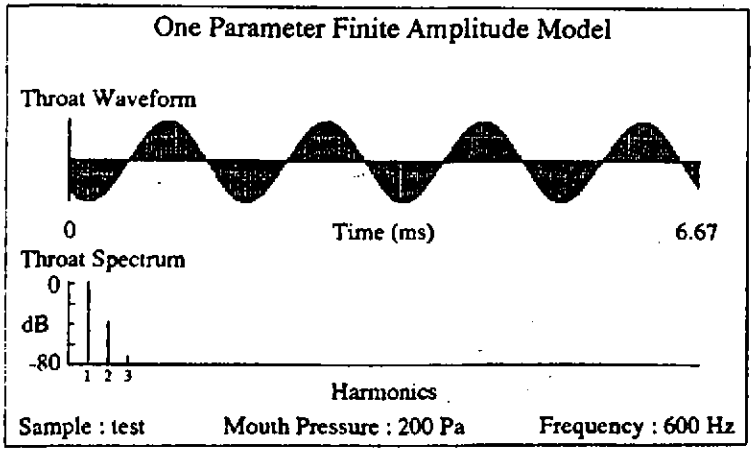

Fig. 3 600 Hz Throat Waveform and Spectrum (model output).

FINITE AMPLITUDE HORN PROPAGATION

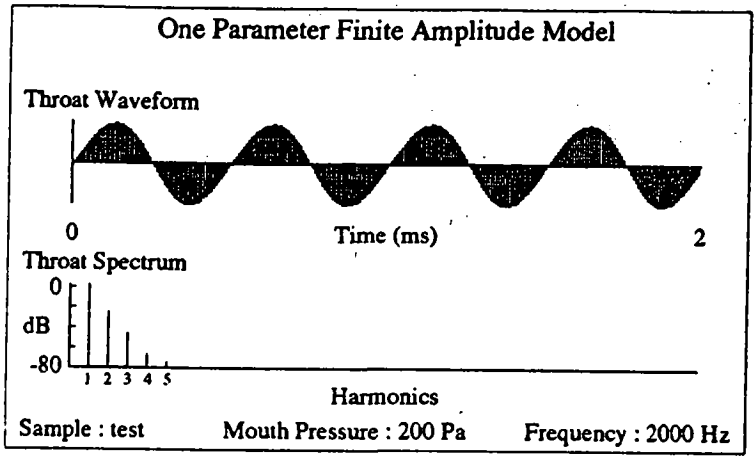

Fig. 4 2000 Hz Throat Waveform and Spectrum (model output).

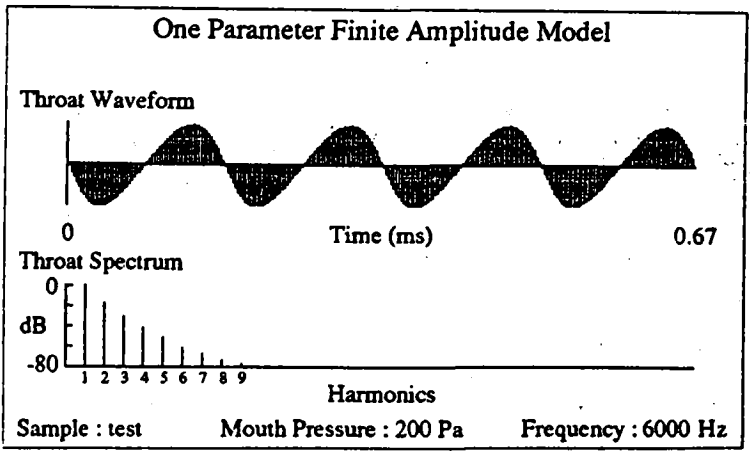

Fig. 5 6000 Hz Throat Waveform and Spectrum (model output).